

RESEARCH PAPER



IGF2BP2 promotes glycolysis and hepatocellular carcinoma stemness by stabilizing CDC45 mRNA via m6A modification

Tao Wu, Li Liao^a, Tao Wu^b, Shuai Chen^b, Qilin Yi^a, and Min Xu^a

^aDepartment of Hepatobiliary Surgery, Yueyang Central Hospital, Yueyang, China; ^bDepartment of Urology Surgery, Yueyang Central Hospital, Yueyang, China

ABSTRACT

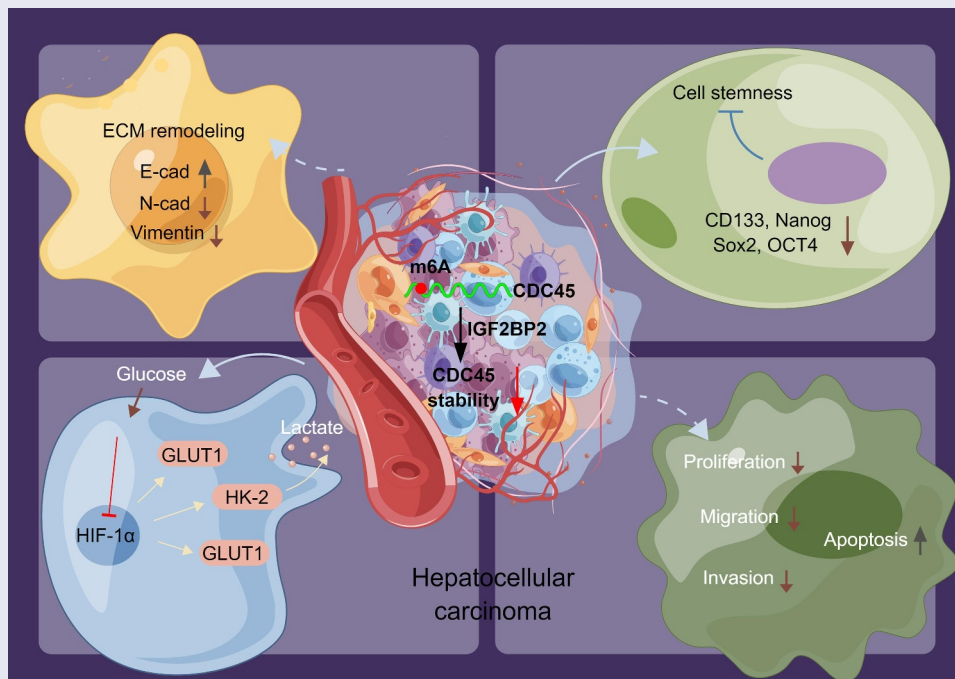
A growing number of studies have shown the prognostic importance of Cell division cycle protein 45 (CDC45) in hepatocellular carcinoma (HCC). This study aims to investigate the biological function and mechanism of CDC45 in HCC. The differential expression and prognostic significance of CDC45 in HCC and normal tissues were analyzed by bioinformatics. CDC45 was knocked down and the biological effects of CDC45 in HCC *in vitro* and *in vivo* were measured. Subsequently, using RNA m6A colorimetry and Methylated RNA Immunoprecipitation (MeRIP), the levels of m6A modification of total RNA and CDC45 were evaluated in cells. RIP was applied to establish that CDC45 and insulin-like growth factor 2 mRNA-binding protein 2 (IGF2BP2) interact. A test using actinomycin D was performed to gauge the stability of the CDC45 mRNA. Furthermore, the regulatory role of IGF2BP2 on CDC45 expression in HCC progression was explored by overexpressing IGF2BP2. High expression of CDC45 was correlated with poor prognosis in HCC patients. Knocking down CDC45 inhibited HCC cell proliferation, migration, invasion, EMT, stemness, and glycolysis, and promoted apoptosis, which was verified through *in vitro* experiments. Additionally, IGF2BP2 was highly expressed in HCC cells, and it was found to interact with CDC45. Knocking down IGF2BP2 resulted in reduced stability of CDC45 mRNA. Moreover, overexpression of IGF2BP2 promoted HCC cell proliferation, migration, invasion, EMT, stemness, and glycolysis, while inhibiting apoptosis, which was reversed by knocking down CDC45. In general, IGF2BP2 promoted HCC glycolysis and stemness by stabilizing CDC45 mRNA via m6A modification.


ARTICLE HISTORY


Received 25 May 2023
Revised 7 October 2023
Accepted 9 October 2023

KEYWORDS

HCC; IGF2BP2; CDC45



CONTACT Min Xu  mintxm0705@sina.com  Department of Hepatobiliary Surgery, Yueyang Central Hospital, No. 39, Dongmaoling Road, Dongmaoling Street, Yueyanglou District, Yueyang, Hunan 414000, China

 Supplemental data for this article can be accessed online at <https://doi.org/10.1080/15384101.2023.2283328>.

© 2023 Informa UK Limited, trading as Taylor & Francis Group

Introduction

Hepatocellular carcinoma (HCC) is accountable for the majority of cancer-related deaths globally and is also the primary cause of cirrhosis-related deaths. Despite progress in HCC therapy, the 5-year relative survival rate for HCC patients remains poor [1–3]. A variety of genetic and epigenetic connections dictate the complicated process of HCC development [4–6]. Hence, uncovering the pathogenesis of HCC is crucial for identifying novel diagnostic biomarkers and therapeutic targets.

The most prevalent mRNA modification in eukaryotic cells is N6-methyladenosine (m6A), which performs essential functions in regulating various mRNA processes including processing, splicing, nucleation, transport, translation, and stability. This modification is crucial for the development of several human diseases, including cancer [7]. Research has established a correlation between m6A and HCC, both in terms of its occurrence and development [8]. Cancer metabolic reprogramming, especially aerobic glycolysis, has become a hallmark of cancer progression [9]. It has been reported that the metabolic reprogramming of HCC cells is induced by HBXIP, which mediates m6A modification of HIF-1 α through METTL3 [10]. Another study reported that CircRHBDD1 enhances HCC glycolysis and limits the efficacy of immunotherapy by promoting m6A reader YTHDF1-mediated PIK3R1 translation [11]. Additionally, abnormal expression of human insulin-like growth factor 2 mRNA binding protein 2 (IGF2BP2), an m6A “reader”, has been linked to excessive cell proliferation and a negative prognosis in HCC [12]. However, whether IGF2BP2 regulates the glycolysis process of HCC remains unclear and needs further study.

Genes involved in the cell division cycle are crucial for life processes, and their dysregulation during cell division may lead to malignant tumors [13]. Cell division cycle 45 (CDC45) is a significant constituent of eukaryotic DNA replicators and performs a crucial function in the CDC45-MCM-GINS (CMG) replicative helicase holoenzyme complex [14]. Prior research

has demonstrated the oncogenic nature of CDC45 in various forms of cancer, including human papillary thyroid carcinoma [15], non-small cell lung cancer [16] and colorectal cancer [17]. Based on transcriptome data and stem cell index co-expression network analysis, it was found that CDC45 is a key biomarker related to HCC stemness characteristics and is linked to a poor prognosis [18,19]. However, the exact mechanism of CDC45 action in HCC is unclear and deserves further exploration.

Given the preceding review, the present article investigates the function and mechanism of CDC45 in HCC by means of bioinformatics analysis, cell studies, and animal experiments. The aim is to offer a useful point of reference for future research on this topic.

Material and methods

Bioinformatics analysis

TCGA dataset in the UCSC Xena database (<https://xenabrowser.net/>) was selected to obtain gene expression and clinical data of 370 HCC patients and 50 nontumor controls. In addition, we also used the ICGC database (<https://dcc.icgc.org/releases/current/Projects/LIRI-JP>) to obtain gene expression and clinical data of 237 HCC patients and 201 nontumor controls. RNA expression profiles were normalized using the DESeq2 package in R software. The expression level of CDC45 mRNA in tumor and normal tissues was compared using an unpaired t-test in GraphPad Prism 8.0 software, with a significance threshold set at $P < 0.05$. We also extracted CDC45 mRNA expression and clinical characteristics of related patients from TCGA and ICGC cohorts, such as survival time and survival status. According to the median expression level of CDC45 mRNA, patients were divided into CDC45 high expression group and CDC45 low expression group. Kaplan-Meier method was used to analyze the overall survival (OS) of the two groups to evaluate the relationship between CDC45 expression and the OS of HCC patients.

Cell culture

The human HCC cell lines SK-Hep-1 (AW-CCH036), HCC-LM3 (AW-CCH210), and HepG2 (AW-CCH024), and normal liver cell line Lx2(AW-CNH008) were purchased from Abiowell (China). Huh7 (CL-0120) was purchased from Pricella (China). SK-Hep-1, HCC-LM3 and HepG2 cells were cultured in MEM (11095080, Gibco, USA). Huh7 cells were cultured in DEME medium (AW-MC002). Lx2 cells were cultured in RPMI-1640 medium (AW-MC002). All medium were supplemented with 10% fetal bovine serum and 1% penicillin-streptomycin. Cells were cultured under 5% CO₂ at 37°C.

Cell transfection

HonorGene (China) designed and synthesized sh-IGF2BP2 (HG-HS1007225) plasmid and oe-IGF2BP2 (HG-HO1007225) plasmid, which were to inhibit and overexpress the target IGF2BP2 gene, respectively. The control plasmids, sh-NC (HG-shNC01) and oe-NC (HG-VPH1305), were purchased from HonorGene. According to the manufacturer's protocol, Lipofectamine 2000 (Invitrogen) was used for transfection. Briefly, the plasmids (5 µl) were added to a sterile tube containing 95 µl of serum-free MEM medium. In a separate tube, 5 µl of Lipofectamine 2000 was added to 95 µl of serum-free MEM medium. After a 5-min incubation at room temperature, the contents of the two tubes were combined and mixed thoroughly. The mixture was added evenly to the cell culture wells to be transfected, ensuring thorough mixing. After a 6-h incubation at 37°C, the complete culture medium was replaced. Cells were collected 48 h post-transfection, and transfection efficiency was checked using qRT-PCR.

Plasmid construction and lentivirus production

sh-CDC45 (HG-HS1178010) and sh-NC (LV-shNC) were cloned into lentiviral vectors and co-transfected it with assistant packaging original plasmids (psPAX2 and pMD2.G) into 293T cells. After 6 h of transfection, the medium was changed

to complete culture medium, and the cells were further cultured for 48 and 72 h. The supernatant was collected to prepare lentiviral particles. SK-Hep-1 cells were seeded in 24-well plates at a density of 5×10^4 [4] cells per well until the confluency reached 70%. The cells were then infected with lentiviral suspension for 48 h, followed by selection using 2 µg/ml puromycin. Forty-eight hours later, puromycin-resistant cells were collected, purified, and amplified. Concurrently, cells were collected, and RNA was extracted for qRT-PCR identification. Cells identified as positive were used for subsequent experiments or seed preservation.

Animal experiment

Male BALB/C nude mice, aged 4 weeks, were obtained from Hunan SJA Experimental Animal Co., Ltd. Following one week of adaptive feeding, the mice were haphazardly allocated to one of two groups: sh-NC or sh-CDC45. The former received subcutaneous injection of SK-Hep-1 cells transfected with sh-NC while the latter received injection of SK-Hep-1 cells transfected with sh-CDC45. Each mouse was injected with 3×10^6 [6] cells in a volume of 150 µl at the left armpit. Tumor volume was monitored biweekly following implantation [20]. 1.25% pentobarbital was administered to put the mice into unconsciousness once the experiment, which lasted 38 days following the tumor injection, was completed. Tumors were excised, and the mice were euthanized. All experimental animals used in this study were handled in accordance with institutional ethical guidelines and approved by the ethical committee of Hunan SJA Laboratory Animal Co., Ltd. (ethical approval number SJA202208011).

Cell counting kit 8 (CCK-8) assay

By allowing the cells to remain in a 0.25% trypsin digestion solution, the cells were separated into a single-cell suspension. The resultant suspension was then seeded with three duplicates of each group and 5×10^4 [3] cells per well onto 96-well plates. Subsequently, the corresponding intervention was performed based on the experimental group. Following a 0, 24, and 48-h culture period, 100 µl

of medium containing CCK-8 (NU679, DOJINDO, Japan) was substituted for the original medium. The cells were then placed in an incubator at a temperature of 37°C, with 5% CO₂ for 4 h. The absorbance was measured at 450 nm using a Bio-Tek microplate reader (MB-530, Heales, China).

Clone formation assay

In the logarithmic growth phase, cells from each group were dissociated and counted. Afterward, cell suspension containing 200 cells per well was injected into each well of a 6-well plate. The plate contained 1 ml of medium for cultivation, which had been brought to room temperature. The cells were cultured at 37°C and 5% CO₂ for 2–3 weeks and the culture was terminated when obvious clones appeared in the culture plate. Subsequently, cells were delicately washed twice with PBS solution after the medium had been discarded. 4% paraformaldehyde (1 mL) was poured into each well and used to fix cell for 15 min. The fixative was discarded, and 1 mL crystal violet staining solution (G1062, Solarbio, China) was added for 30 min. The samples were air-dried and photographed following a thorough washing of the background dye under running water to eliminate the staining solution.

Wound healing assay

A 6-well plate was taken and a horizontal line was drawn evenly behind the plate. Following dissociation, the cells were counted and seeded into 6-well plates at a concentration of 5×10^5 [5] cells/well. After the plate were covered with cells, scratches were made perpendicular to the previous horizontal line. Cell debris was removed with PBS. DMEM medium with low serum (5%) was added and cultured at 37°C, under 5% CO₂. The scratch widths were observed and recorded at 0, 24, and 48 h using an inverted biological microscope (DSZ2000X, Cnmicro, China), with three fields of view taken at each time point. The narrower the scratch width, the stronger the cell migration capability.

Sphere formation assay

Cells underwent processing to form a single-cell suspension which was then distributed into ultra-low attachment 24-well plates (Costar). Approximately 2×10^6 [6] cells were cultured in a growth medium devoid of serum, but enriched with 1:50 B27, EGF (20 ng/ml), essential fibroblast growth factor (20 ng/ml) and heparin (10 µg/ml). The plate was incubated at 37°C, 5% CO₂ for 10 days, after which the number of spheres was quantified and imaged [21].

Transwell assay

The upper chamber was precoated with Matrigel and incubated at 37°C for 30 min to allow gelling. The cells were treated with trypsin and then resuspended in serum-free medium at a concentration of 2×10^6 [6] cells/ml before being seeded into the upper chamber. The lower chamber was filled with 500 µl of culture medium containing 10% FBS. After incubating for 48 h at 37°C with 5% CO₂, the cells in the upper chamber were removed using a cotton swab. The invaded cells were then fixed with 4% paraformaldehyde for 20 min and stained with 0.1% crystal violet for 5 min. Following a rinse with PBS, three random fields were selected under a microscope and photographed for observation and counting.

Flow cytometry

To assess cell apoptosis, the FITC apoptosis kit (KGA1030, KeyGen, China) was used. Cells were digested with trypsin (without EDTA) and collected as a single-cell suspension. A total of 3.2×10^6 [5] cells were collected and then suspended in binding buffer (500 µl) following a 5-min centrifugation at 2000 rpm. Subsequently, a mixture was prepared by combining cell suspension with 5 µl each of Annexin V-FITC and Propidium Iodide, and incubation of the resultant mixture in the dark for 10 min followed. Within one hour, analysis of the cell apoptosis was conducted using flow cytometry (A00-1-1102, Beckman, USA).

qRT-PCR

To extract RNA, tissue/cells were lysed using TRIzol (15596026, Thermo, USA) for 3 min.

Table 1. Primer sequences.

Target Gene	Primer Sequences	Amplicon Length
β -actin	FACCCTGAAGTACCCCATCGAG RAGCACAGCCTGGATAGCAAC	224 bp
CDC45	FGGTGATCCTGGACCAATCG RGAGGCCACGAAGAGAAGGAC	180 bp
IGF2BP2	FTTACATCGGGAACCTGAGCC RCAGCTTCTGTCCCAAAGA	70 bp

Following that, 200 μ l of chloroform was added, shaken for 15 s, and settled for 3 min before centrifugation. The upper aqueous phase was collected and combined with an equal volume of isopropanol at room temperature for 10 min. After centrifugation, the supernatant was discarded, and the RNA pellet was washed with 1 mL of 75% ethanol. The RNA pellet was air-dried for 5–10 min before being reconstituted with 20–30 μ l of RNase-free water. The RNA purity was assessed using a NanoDrop 2000 spectrophotometer (Thermo, USA), and the RNA integrity was evaluated through agarose gel electrophoresis and Agilent 2100 Bioanalyzer system (Agilent Technologies, USA) to ensure the accuracy and validity of the experimental results. cDNA was synthesized using an mRNA reverse transcription kit (CW2569, CWBIO, China) by reverse transcribing mRNA. The reaction system consisted of 2 μ g of RNA, 4 μ l of 5 \times RT Buffer, 4 μ l of dNTP Mix (500 μ M), 2 μ l of RT Primer Mix (0.2 μ M), 2 μ l of DTT (10 mM), and 1 μ l of HiFiScript (200 U/uL), with a total volume of 20 μ l and a concentration of 0.25 μ g/ μ l. The reaction mixture was incubated at 50°C for 50 min, followed by 85°C for 5 min. For qRT-PCR amplification, Ultra SYBR Mixture (CW2601, CWBIO, China) and specific primer combinations were used, and each reaction contained 100 ng of cDNA. PCR was performed in the QuantStudio1 qRT-PCR apparatus (QuantStudio1, Thermo, USA), involving an initial denaturation at 95°C for 10 min, followed by 40 amplification cycles at 95°C for 15 s and 60°C for 30 s. Post-run melting curve analysis was conducted to confirm a single product generation. Relative expression levels of target genes were determined using the $2^{-\Delta\Delta C_t}$ calculation method with β -actin serving as the internal reference gene. Table 1 represents the primer sequences employed in this investigation.

Western blot (WB)

To obtain protein samples, cells and tissues were treated with RIPA lysis buffer (AWB0136, Abiowell, China) as directed. The protein concentrations of each group were quantified using the BCA protein assay kit (BL521A, Biosharp, China). The supernatant containing protein after electrophoresis separation was then transferred to a nitrocellulose membrane, which was subsequently blocked at room temperature for 1.5 h with 5% skimmed milk powder. Primary antibodies targeting CDC45 (15678–1-AP, 1: 500, Proteintech, USA), IGF2BP2 (11601–1-AP, 1: 5000), N-cadherin (N-cad; 22018–1-AP, 1: 5000), Vimentin (10366–1-AP, 1: 5000), E-cadherin (E-cad; 20874–1-AP, 1:5000), CD133 (-18470–1-AP, 1: 5000), Nanog (14295–1-AP, 1: 1500), SOX2 (11064–1-AP, 1: 600), OCT4 (11263–1-AP, 1: 3000), HIF-1 α (ab179483, 1: 1000, Abcam, UK), HK-2 (22029–1-AP, 1: 4000), GLUT1 (21829–1-AP, 1: 4000), PKM2 (15822–1-AP, 1: 4000), and β -actin (66009–1-Ig, 1: 5000), were incubated with the membrane overnight at 4°C. HRP goat anti-mouse IgG (SA00001–1,1: 5000) and HRP goat anti-rabbit IgG (SA00001–2,1: 6000) were incubated for 1.5 h at room temperature. Apart from HIF-1 α , all the other antibodies were provided by Proteintech (USA). The washed samples were analyzed using ECL color exposure and Odyssey software to determine the intensity of the band.

Global mRNA m6A methylation

To determine the global m6A methylation levels, the m6A RNA Methylation Quantification Kit (Colorimetric) from Abcam (ab185912) was utilized following the manufacturer's protocol. Specifically, the RNA sample was treated with an alkaline hydrolysis enzyme, and then loaded onto a capture substrate stick. Subsequently, m6A antibody (ab286164, Abcam, UK) were added to the substrate stick to detect m6A methylation levels. After washing with buffer, a chromogenic medium was added to produce a colorimetric signal. Finally, the intensity of the color reaction was measured using a spectrophotometer to calculate the m6A content in the RNA sample.

Methylated RNA immunoprecipitation PCR (MeRIP-PCR)

The Magna MeRIP m6A Kit from Millipore was utilized to measure the level of m6A modification in CDC45 mRNA. RNA fragments were combined with m6A antibody to form RNA-antibody complexes, which were then captured using protein A beads. And the samples were incubated at 4°C for 10 h to facilitate the formation and stability of the complexes. Protein-RNA complexes were washed, proteinase K was added, and the immunoprecipitated RNA level was quantified using qRT-PCR.

RIP assay

To perform RIP analysis, the Magna RIP kit from Millipore was used along with IGF2BP2 (11601-1-AP, Proteintech, USA) or IgG (ab48386, Abcam, UK) antibodies. Cell lysates were prepared from 1×10^6 cells using 100 μ l of RIP lysis buffer, and incubated with magnetic beads conjugated with IGF2BP2 antibody or IgG at 4°C for 12 h. Afterward, RNA was isolated, purified, and eluted. The level of precipitated RNA was obtained using qRT-PCR.

Actinomycin D experiment

Using the actinomycin D test, the stability of mRNA in cells was examined. Briefly, mRNA was collected for qRT-PCR analysis after cells were treated with 5 μ g/mL actinomycin D for 0, 2, 4, 6, and 8 h [22].

Biochemical detection

To measure the concentrations of glucose, lactic acid, and ATP, a set of detection kits were utilized, including the glucose detection kit (F006-1, Sigma-Aldrich), the fluorescent lactic acid detection kit (A019-2-1), and the luminescent ATP detection kit (A095-1-1). Except for the glucose detection kit, all other kits were procured from Nanjing Jiancheng Bioengineering Institute.

Haematoxylin-eosin (HE) staining

To prepare tissue samples for observation, 6 μ m-thick sections of paraffin-embedded tissue were dehydrated using graded concentrations of ethanol and xylene. After a 1-min hematoxylin staining, the sections were rinsed with distilled water and blue-shaded using PBS. Eosin staining was then applied for 1 min followed by a 5-min alcohol gradient dehydration step (95%-100%). The sections were then treated with xylene for 10 min before being sealed with neutral gum. Observation was carried out using a microscope.

Statistical analysis

Utilizing GraphPad Prism 8, statistical analysis was carried out. For each experiment, we performed three repetitions and three independent trials to ensure accuracy and reliability of the data. The Shapiro-Wilk test and Levene test was applied to check the normality and homogeneity of variance of the data. The measurement data are expressed as mean \pm standard deviation. The unpaired t-test was utilized to compare two experimental groups, while the one-way analysis of variance (ANOVA) was used to compare differences among more than two groups. A significance level of $P < 0.05$ was applied.

Results

Association between high expression of CDC45 and poor prognosis in HCC patients

To begin with, we evaluated the potential association between CDC45 and HCC prognosis by predicting the expression of CDC45 in HCC and normal tissues. We analyzed mRNA expression data on CDC45 in HCC patients from UCSC Xena and ICGC databases and analyzed the results via a box plot. As illustrated in Figure 1(a,b), the expression level of CDC45 was markedly higher in HCC patients than in the healthy. Moreover, patients with high CDC45 expression exhibited poorer survival rates than those with low expression, according to Kaplan-Meier survival curves (Figure 1c,d). Furthermore, we utilized qRT-PCR to quantify CDC45 expression in LX2 cells and four human HCC cell lines. As illustrated in Figure 1e, CDC45

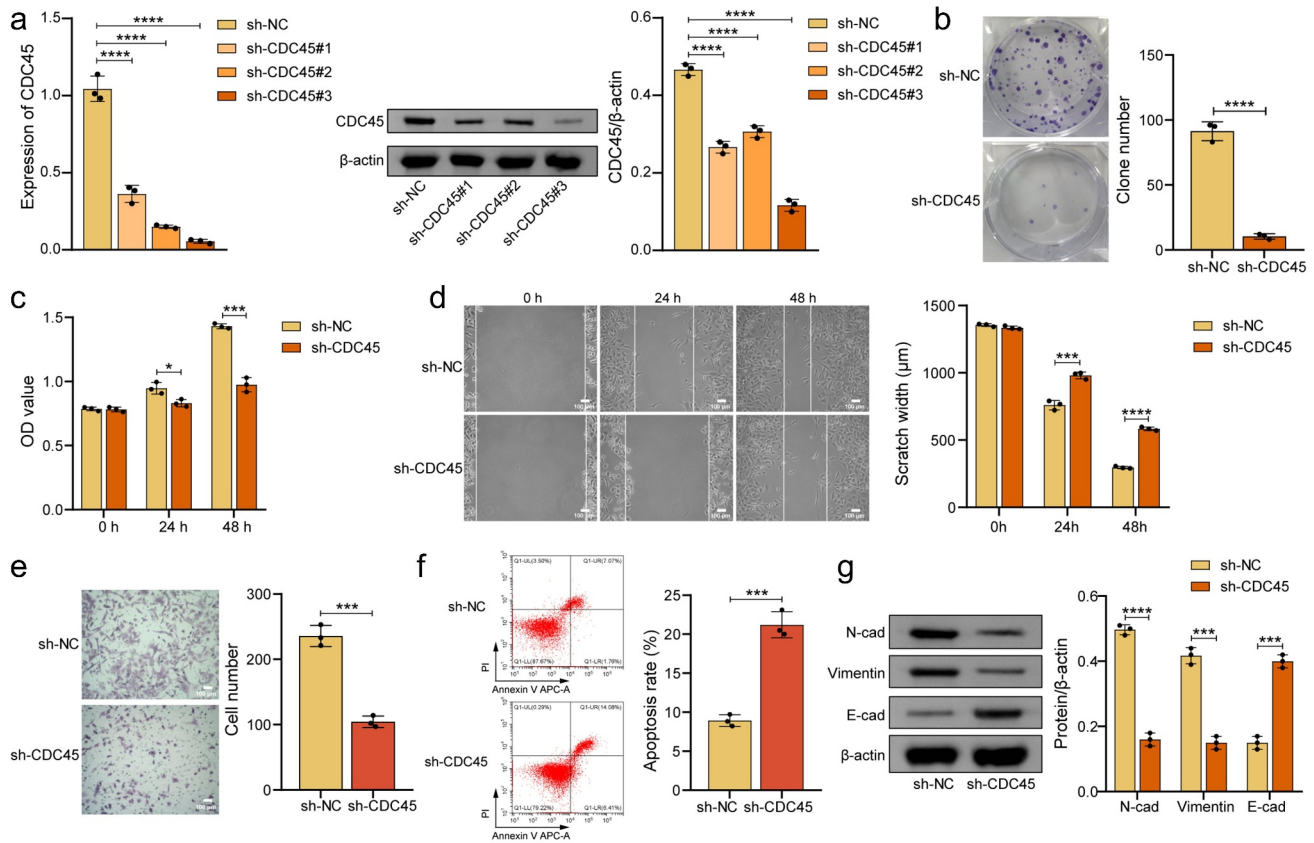


Figure 2. Knockdown of CDC45 inhibited HCC cell proliferation, migration, invasion and EMT, while promoting apoptosis. (a) qRT-PCR and WB methods were utilized to detect the expression levels of CDC45 in SK-Hep-1 cells transfected with sh-CDC45#1, sh-CDC45#2, and sh-CDC45#3. Notably, sh-CDC45#3 demonstrated the most pronounced inhibitory effect on CDC45. (b) the results of the colony formation assay demonstrated a pronounced reduction in the number of colonies formed by SK-Hep-1 cells transfected with sh-CDC45, as compared to the sh-NC group. (c) CCK-8 experiments revealed a significant decrease in proliferation ability in SK-Hep-1 cells transfected with sh-CDC45, in comparison to the sh-NC group. (d) wound healing test showed a significant reduction in the migration ability of SK-Hep-1 cells transfected with sh-CDC45 compared to the sh-NC group. (e) Transwell assay results exhibited a prominent attenuation of invasive capacity in SK-Hep-1 cells transfected with sh-CDC45, as compared to the sh-NC group. (f) flow cytometry analysis showed a substantial increase in apoptosis in SK-Hep-1 cells transfected with sh-CDC45, relative to the sh-NC group. (g) WB analysis indicated a substantial increase in E-cad protein expression and a significant decrease in N-cad and Vimentin protein expression in SK-Hep-1 cells transfected with sh-CDC45, relative to the sh-NC group. * $P < .05$, ** $P < .01$, *** $P < .001$, **** $P < .0001$.

expression was highest in SK-Hep-1 cells. Therefore, we chose to concentrate our study on SK-Hep-1 cells in further studies. Overall, our findings suggested that HCC patients with high CDC45 expression had a worse prognosis.

Knockdown of CDC45 inhibited HCC cell proliferation, migration, invasion and epithelial-mesenchymal transition, while promoted apoptosis

To investigate the impact of CDC45 on HCC cell proliferation, migration, invasion, and apoptosis, we constructed three shRNAs targeting CDC45 to knockdown its expression. We validated their

effectiveness relative to sh-NC through qRT-PCR and Western blotting (Figure 2a). Among them, sh-CDC45#3 exhibited a higher knockdown efficiency compared to sh-CDC45#1 and sh-CDC45#2, which was used for subsequent experiments. We employed clone formation assays and CCK-8 experiments to evaluate cell proliferation, and the findings indicated that cell proliferation was lower in the sh-CDC45 group than in the sh-NC group within 48 h (Figure 2b,c). The data in Figure 2d–f demonstrated that HCC cells exhibited reduced invasion and migration abilities alongside higher apoptosis rates in the sh-CDC45 group versus the sh-NC group. WB analyses were performed to identify expression levels of EMT

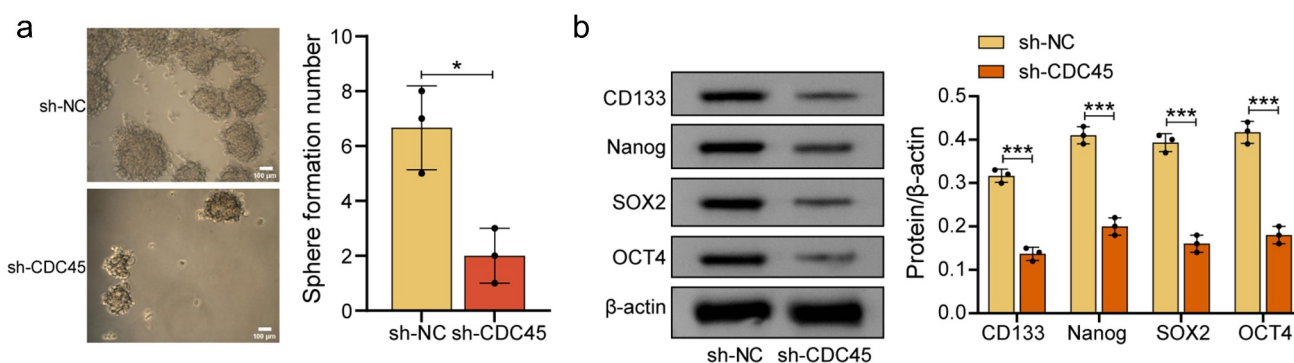


Figure 3. Knockdown of CDC45 inhibited HCC cell stemness. (a) the sphere formation assay demonstrated a significantly lower SFE in SK-Hep-1 cells transfected with sh-CDC45 compared to the sh-NC group. (b) WB analysis revealed significant decreases in the protein expression levels of CD133, Nanog, SOX2, and OCT4 in SK-Hep-1 cells transfected with sh-CDC45 compared to the sh-NC group. * $P < .05$, ** $P < .01$, *** $P < .001$, **** $P < .0001$.

biomarkers, and the findings revealed that expression of E-cad increased while N-cad and Vimentin expression levels decreased in the sh-CDC45 group compared to the sh-NC group (Figure 2g). Generally, our investigations revealed that knockdown of CDC45 inhibited HCC cell proliferation, migration and invasion and promoted apoptosis, along with probably impeding EMT.

Knockdown of CDC45 inhibited HCC cell stemness

We also evaluated the impact of CDC45 on the stemness of HCC cells. Our results from sphere formation assays demonstrated that HCC cells in the sh-CDC45 group exhibited a lower sphere-formation efficacy (SFE) than those in the sh-NC group (Figure 3a). Otherwise, we utilized WB to detect stem-cell surface marker expression and found that the levels of CD133, Nanog, SOX2, and OCT4 were lower in the sh-CDC45 group compared to the sh-NC group (Figure 3b). The foregoing findings illustrated that CDC45 knockdown impeded HCC cell stemness.

Knockdown of CDC45 inhibited glycolysis in HCC cells

It is worth mentioning that reprogramming of glycolysis is a known hallmark of cancer metabolism. Hence, we decided to evaluate the role of CDC45 in the glycolysis of HCC cells. Our findings (illustrated in Figure 4a) indicated that the expression of genes

involved in glycolysis, such as HIF-1 α , HK-2, GLUT1, and PKM2, was lower in the sh-CDC45 group in comparison with the sh-NC group. Furthermore, lactic acid and ATP levels were substantially lower in the sh-CDC45 group compared to the sh-NC group, while the remaining glucose levels in the culture medium were the opposite (Figure 4b–d). These findings revealed that knockdown of CDC45 inhibited glycolysis in HCC cells.

Knockdown of CDC45 inhibits HCC progression in vivo

Our study also sought to validate the impact of CDC45 on HCC progression *in vivo*. As demonstrated in Figure 5a–c, tumor volume and weight in the sh-CDC45 group were relatively lower than sh-NC group. HE staining revealed a decrease in tumor cells and an increase in necrotic cells in the sh-CDC45 group, in contrast to the sh-NC group (Figure 5d). Additionally, qRT-PCR and WB analyses revealed reduced CDC45 expression levels in the sh-CDC45 group as compared to the sh-NC group, signifying successful construction of a CDC45-knockdown mouse model *in vivo* (Figure 5e). In line with this, WB was also carried out to evaluate EMT-related markers, stem cell surface markers, and glycolysis-related genes in both groups of mice. The outcomes indicated that the expression levels of N-cad, Vimentin, CD133, Nanog, SOX2, OCT4, HIF-1 α , HK-2, GLUT-1, and PKM2 were reduced, whereas E-cad expression increased in the sh-CDC45

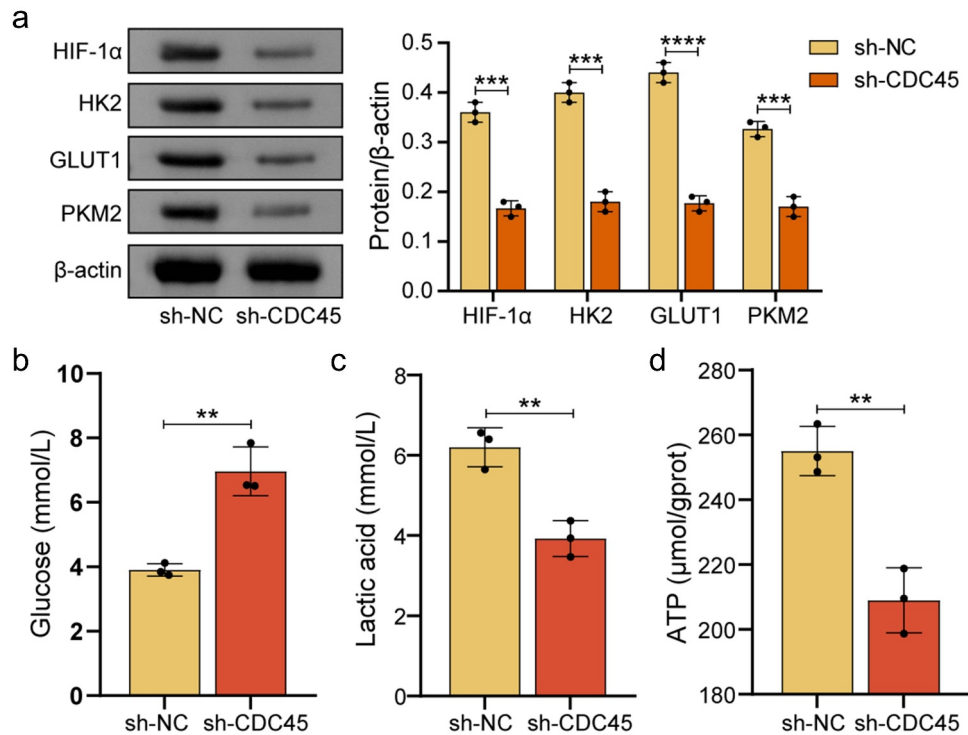


Figure 4. Knockdown of CDC45 inhibited glycolysis in HCC cells. (a) WB analysis revealed a significant decrease in the expression levels of HIF-1α, HK-2, GLUT1, and PKM2 in SK-Hep-1 cells transfected with sh-CDC45 compared to the sh-NC group. (b-d) biochemical analysis demonstrated a significant decrease in glucose uptake, lactate release, and ATP generation in SK-Hep-1 cells transfected with sh-CDC45 compared to the sh-NC group. * $P < .05$, ** $P < .01$, *** $P < .001$, **** $P < .0001$.

group, as opposed to the sh-NC group (Figure 5f-h). Our data indicated that CDC45 knockdown impeded HCC progression *in vivo*.

IGF2BP2 affected the stability of CDC45 mRNA

In order to comprehend the underlying mechanism of CDC45 affecting HCC progression, we conducted investigations into the involvement of m6A methylation. Firstly, we measured the m6A methylation level of total RNA and CDC45 via colorimetry and MeRIP, respectively. Our observations revealed that the m6A methylation level of total RNA and CDC45 in LX2 cells were lower in comparison to those in SK-Hep-1 cells (Figure 6a,b). Subsequently, we utilized WB to study the differential expression of m6A binding proteins, including METTL3, YTHDF1, YTHDC1, IGF2BP1, IGF2BP2, and IGF2BP3, in LX2 and SK-Hep-1 cells. As depicted in Figure 6c, we noted higher expression levels of these proteins in SK-Hep-1 cells, particularly IGF2BP2. Our findings also indicated the interaction between IGF2BP2 and CDC45

mRNA (Figure 6d). To further explore the regulatory relationship between IGF2BP2 and CDC45, we intervened with IGF2BP2 expression. As demonstrated in Figure 6e, the knockdown efficiency of sh-IGF2BP2#2 was found to be higher than that of sh-IGF2BP2#1 and sh-IGF2BP2#3, and thus it was used for subsequent experiments. Subsequent Actinomycin D analysis demonstrated that CDC45 mRNA stability was lower in the sh-IGF2BP2 group than in the sh-NC group (Figure 6f). Additionally, we found that the interaction between IGF2BP2 and CDC45 mRNA and the stability of CDC45 mRNA was lower in the sh-IGF2BP2 group relative to the sh-NC group (Figure 6g,h), indicating that IGF2BP2 played a critical role in maintaining the stability of CDC45 mRNA.

Knockdown of CDC45 reversed the promotion of IGF2BP2 on proliferation, migration, invasion, EMT, stemness and glycolysis of HCC cells

Finally, we aimed to investigate the regulatory function of CDC45 and IGF2BP2 in HCC cell

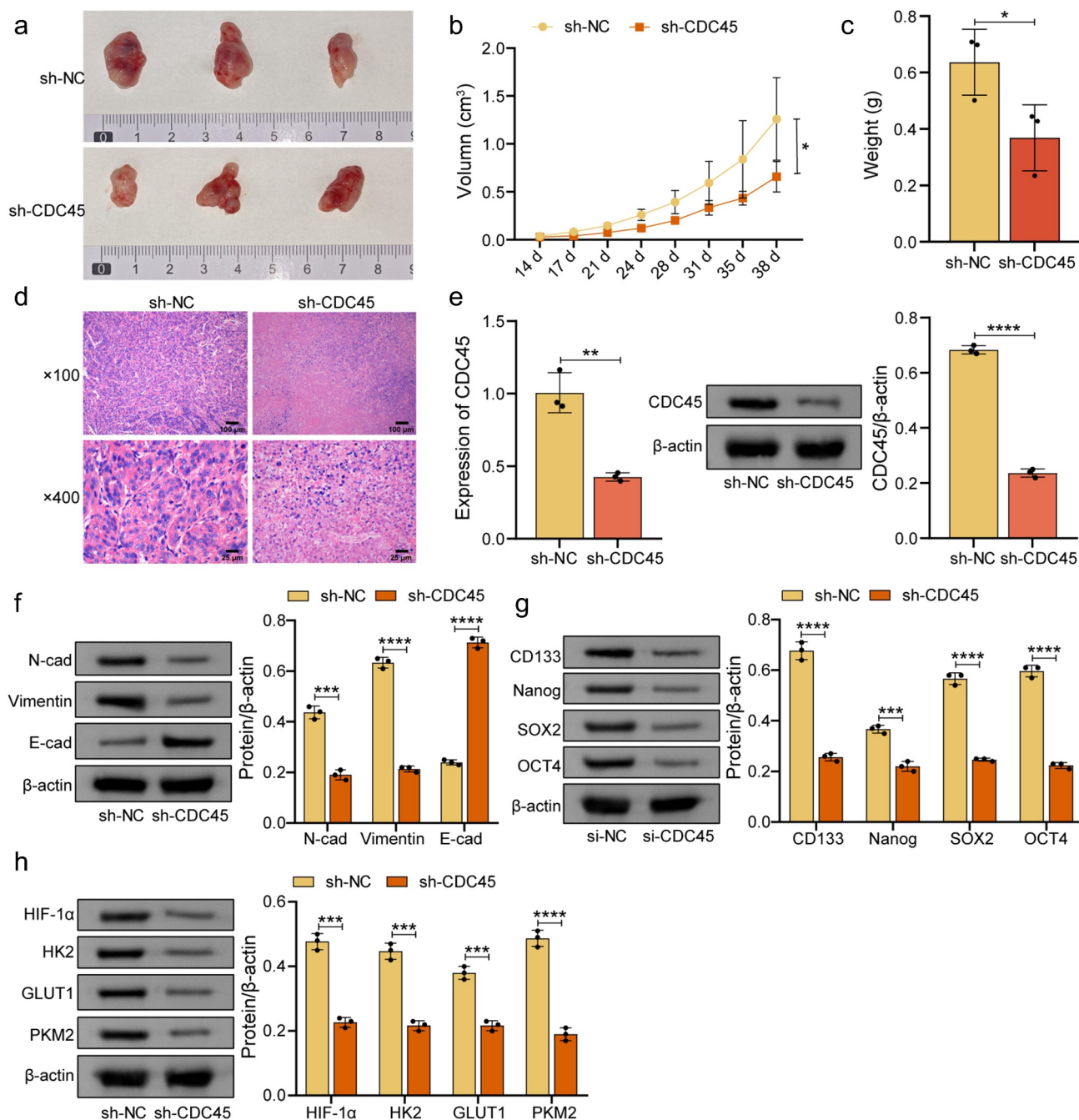


Figure 5. Knockdown of CDC45 inhibited HCC progression *in vivo*. (a) images of tumors in nude mice from the sh-NC and sh-CDC45 groups on day 38. (b) growth volume curve of tumors in nude mice from the sh-NC and sh-CDC45 groups. Tumor volume was significantly smaller in the sh-CDC45 group compared to the sh-NC group. (c) tumor weight on day 38 was significantly lower in the sh-CDC45 group compared to the sh-NC group. (d) HE staining revealed a decrease in tumor cell and an increase in necrotic cells in the sh-CDC45 group compared to the sh-NC group. (e) qRT-PCR and WB analysis showed a decreased expression of CDC45 in tumor tissues from the sh-CDC45 group compared to the sh-NC group. (f-h) WB analysis revealed a significant increase in E-cad protein expression, and a significant decrease in N-cad, Vimentin, CD133, Nanog, SOX2, OCT4, HIF-1 α , HK-2, GLUT-1, and PKM2 protein expression in the sh-CDC45 group compared to the sh-NC group. * $P < .05$, ** $P < .01$, *** $P < .001$, **** $P < .0001$.

proliferation, migration, invasion, EMT, stemness, and glycolysis. IGF2BP2 was overexpressed while CDC45 was knocked down (Figure 7a). Compared to the oe-NC group, cell proliferation, migration,

and invasion abilities were increased in the oe-IGF2BP2 group, while the apoptosis rate decreased. However, sh-CDC45 counteracted the effects of oe-IGF2BP2 on these indexes (Figure 7B-

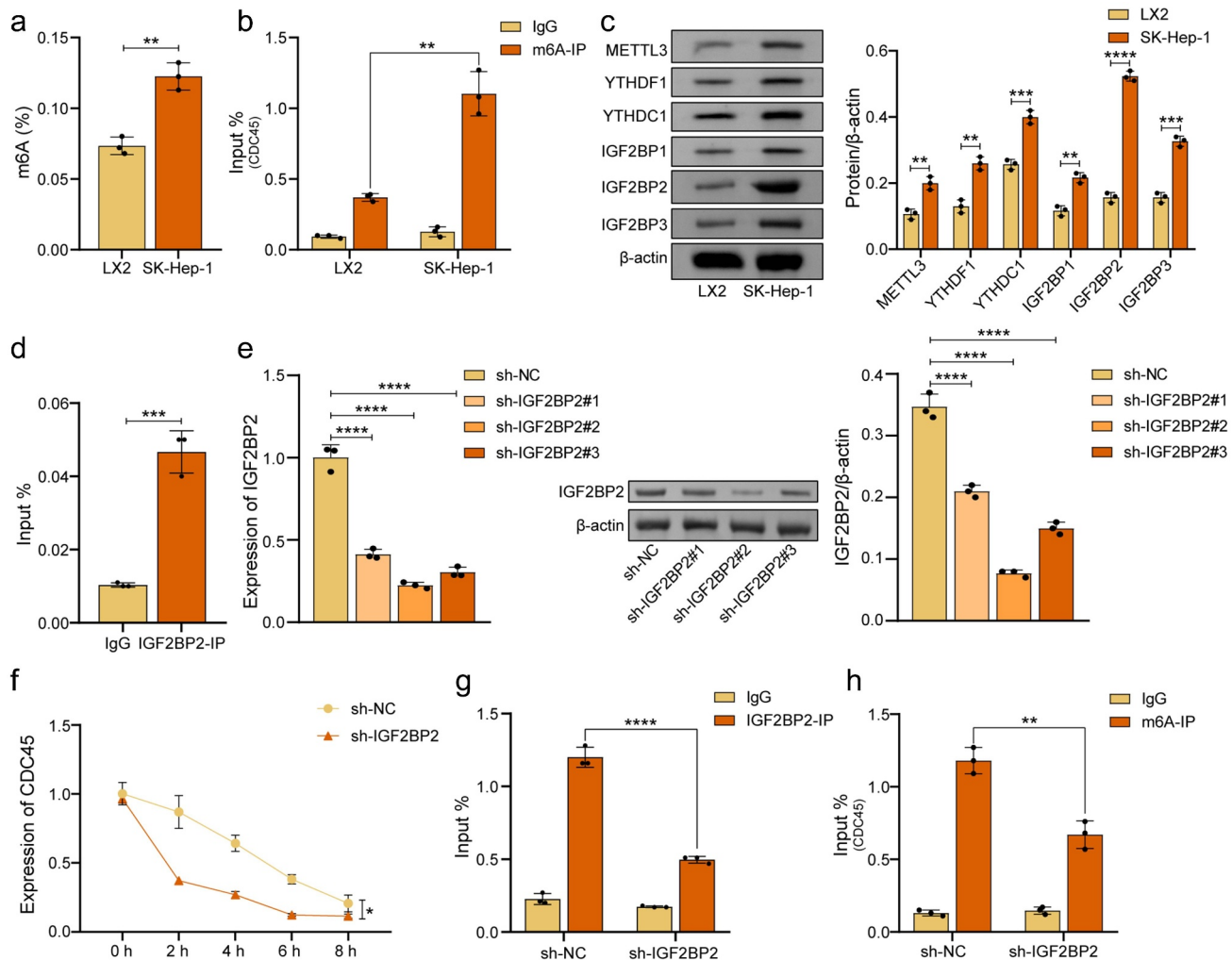


Figure 6. IGF2BP2 affected the stability of CDC45 mRNA. (a) comparative analysis of colorimetric assays revealed an increase in m6A methylation levels within the total RNA of SK-Hep-1 cells when compared to LX2 cells. (b) MeRIP detection findings indicated a remarkable elevation in m6A modification levels of CDC45 in SK-Hep-1 cells in contrast to LX2 cells. (c) WB analysis exhibited notable upregulation of protein expressions of METTL3, YTHDF1, YTHDC1, IGF2BP1, IGF2BP2, and IGF2BP3 in SK-Hep-1 cells, with IGF2BP2 displaying the most significant enhancement, in comparison to LX2 cells. (d) through RIP experiments, the interaction between IGF2BP2 and CDC45 mRNA was confirmed in SK-Hep-1 cells. (e) both qRT-PCR and WB analysis demonstrated a reduction in IGF2BP2 expression in SK-Hep-1 cells with transfection of sh-IGF2BP2#1, sh-IGF2BP2#2, and sh-IGF2BP2#3, with the most substantial knockdown observed in sh-IGF2BP2#2. (f) analysis using the actinomycin D assay revealed a significant decrease in mRNA stability in SK-Hep-1 cells that were transfected with sh-IGF2BP2 compared to the sh-NC group. (g) RIP technique validated a decrease in the interaction between IGF2BP2 and CDC45 in SK-Hep-1 cells transfected with sh-IGF2BP2. (h) MeRIP detection unveiled a considerable reduction in m6A modification levels of CDC45 in SK-Hep-1 cells transfected with sh-IGF2BP2 in comparison to the sh-NC group. * $P < .05$, ** $P < .01$, *** $P < .001$, **** $P < .0001$.

7F). Additionally, sphere formation assay data revealed that SFE of HCC cells in the oe-IGF2BP2 group was substantially greater than that in the oe-NC group, but this was reversed after further knockdown of CDC45 (Figure 7h). Using WB, EMT-related indicators, stem cell surface markers, and glycolysis-related genes for each group were detected. The findings demonstrated that in comparison with the oe-NC group, expression of N-cad, Vimentin, CD133, Nanog, SOX2,

OCT4, HIF-1 α , HK-2, GLUT1 and PKM2 in the oe-IGF2BP2 group increased, while E-cad expression decreased. Knockdown of CDC45 reversed the effects of oe-IGF2BP2 on these indicators (Figure 7g, i-j). As shown in Figure 7K-7M, the levels of lactic acid and ATP were significantly higher in the oe-IGF2BP2 group than in the oe-NC group. In contrast, the remaining glucose levels in the culture medium were lower, and knocking down CDC45 reversed the effects of oe-

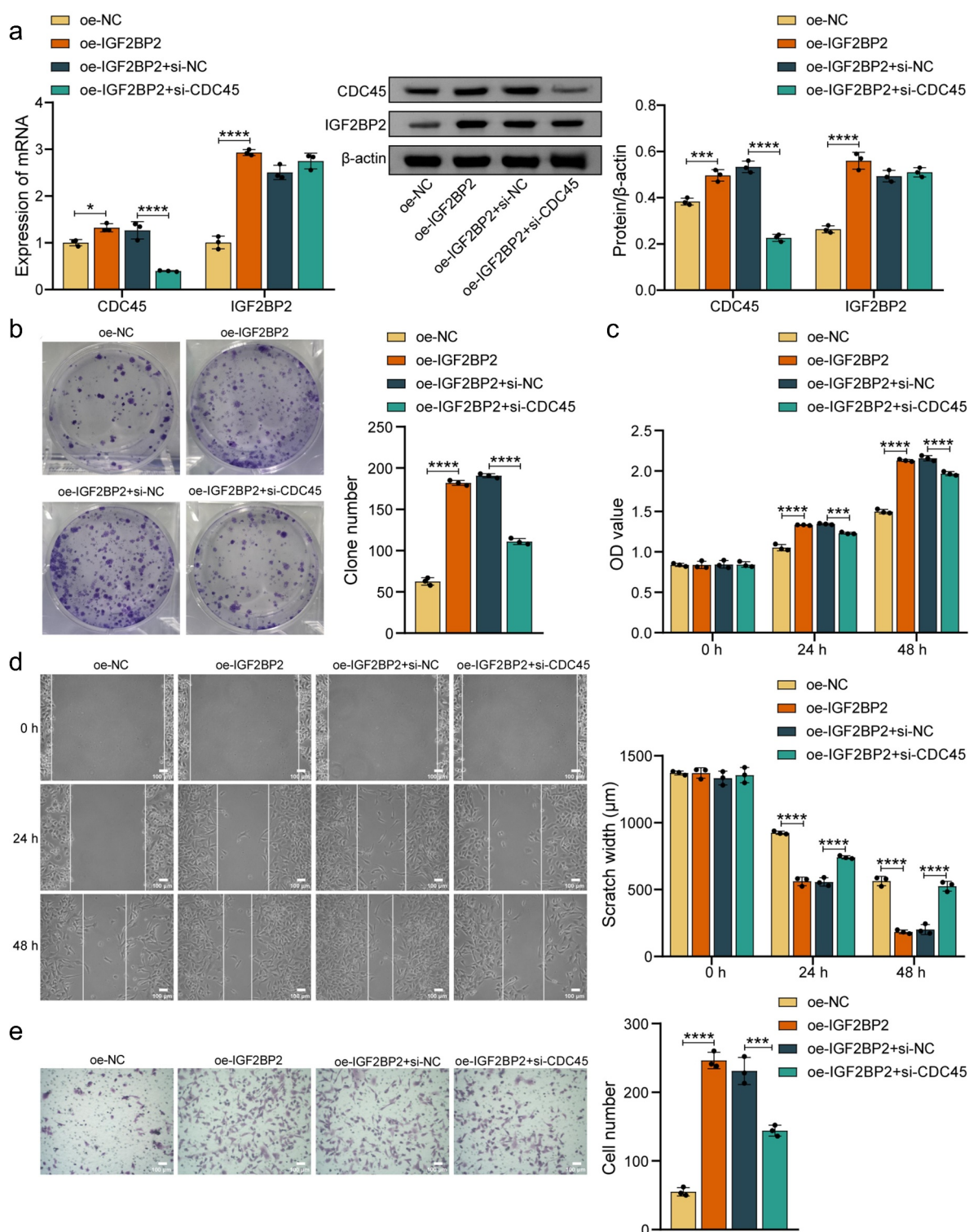


Figure 7a. Knockdown of CDC45 reversed the promotion by IGF2BP2 of HCC cell proliferation, migration, invasion, EMT, cell stemness and glycolysis. (a) SK-Hep-1 cells transfected with oe-IGF2BP2 and sh-CDC45 were subjected to qRT-PCR and WB analysis to assess the expression of IGF2BP2 and CDC45. (b) sh-CDC45 reversed the promotive effect of oe-IGF2BP2 on colony formation in SK-Hep-1 cells. (c) the proliferative effect of oe-IGF2BP2 on SK-Hep-1 cells was reversed by sh-CDC45, as shown by CCK-8 assay. (d) wound healing assay results demonstrated that sh-CDC45 reversed the promoting effect of oe-IGF2BP2 on the migration of SK-Hep-1 cells. (e) the promotive effect of oe-IGF2BP2 on cell invasion in SK-Hep-1 cells was reversed by sh-CDC45, according to the transwell assay results. (f) flow cytometry analysis showed that the inhibitory effect of oe-IGF2BP2 on apoptosis in SK-Hep-1 cells was reversed by sh-CDC45. (g) WB analysis indicated that oe-IGF2BP2 promoted the expression of N-cad and vimentin proteins and inhibited E-cad expression in SK-Hep-1 cells, which was reversed by sh-CDC45. (h) sphere formation assay results demonstrated that sh-CDC45

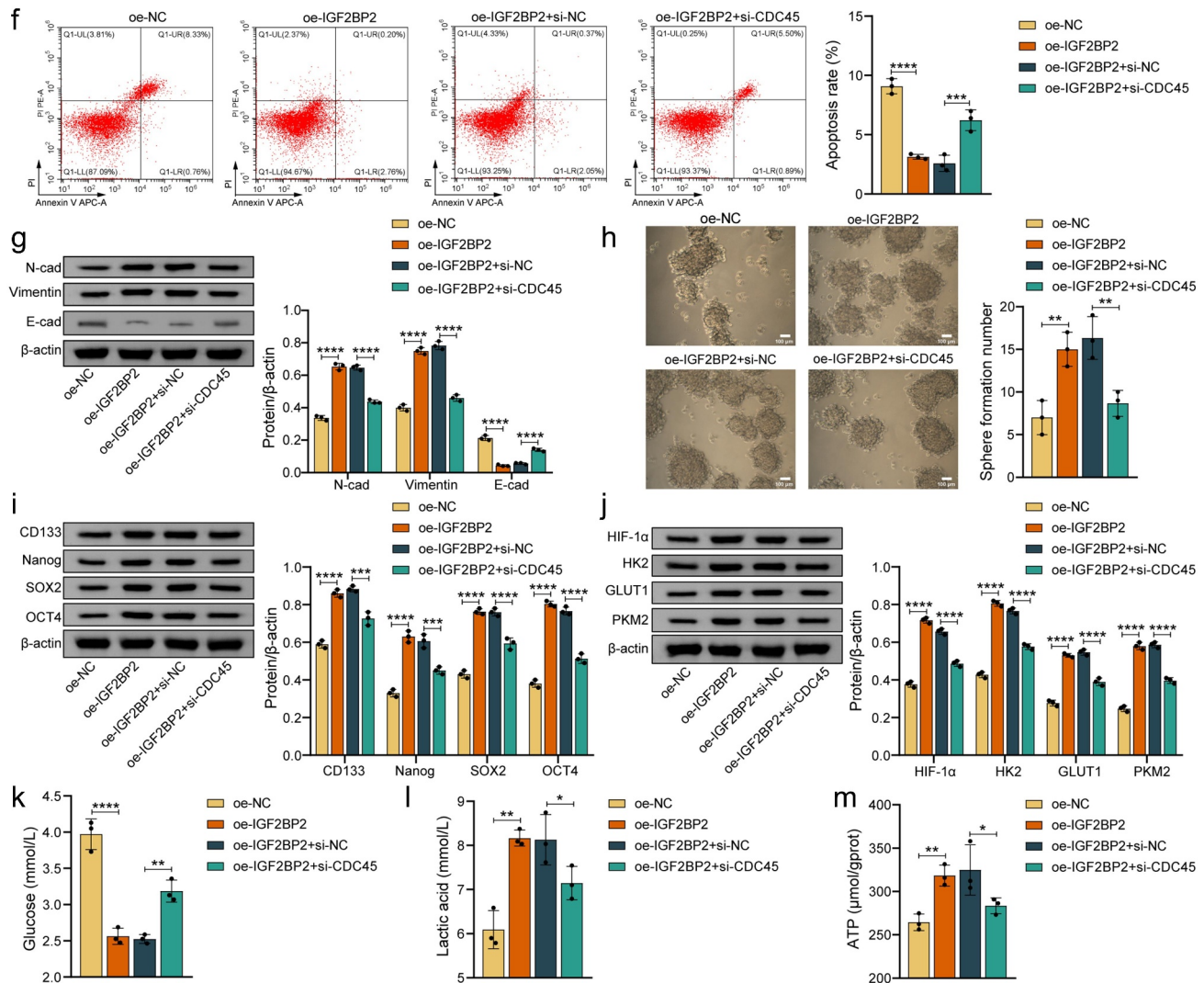


Figure 7b. (Continued).

IGF2BP2 on these indicators. These results showed that knockdown of CDC45 abolished the promotion of IGF2BP2 on HCC cell proliferation, migration, invasion, apoptosis, EMT, stemness, and glycolysis, as well as the inhibition of apoptosis.

Discussion

HCC poses a significant public health burden, being the leading cause of cancer-related fatalities globally [2,3]. Furthermore, CDC45's involvement in HCC

development has been established, with high levels of the protein correlating to worse outcomes in HCC patients [18,19]. Our research revealed elevated CDC45 expression in HCC tissue, CDC45 knockdown impeded HCC progression, and IGF2BP2 impacted cell stemness, glycolysis, invasion, migration, EMT, proliferation and apoptosis by preserving m6A modification of CDC45. To our knowledge, the mechanism by which CDC45 acts in HCC has not been previously reported, which is also the innovation of this research.

reversed the promotion of sphere-forming ability in SK-Hep-1 cells induced by oe-IGF2BP2. (i) and (j) WB analysis showed that sh-CDC45 counteracted the promotion of surface markers (CD133, Nanog, SOX2, and OCT4) and glycolysis-related genes (HIF-1 α , HK-2, GLUT1, and PKM2) protein expression by oe-IGF2BP2 in SK-Hep-1 cells. (k) (l) and (m) biochemical analysis results indicated that sh-CDC45 reversed the promoting effects of oe-IGF2BP2 on glucose uptake, lactate release, and ATP generation in SK-Hep-1 cells. * $P < .05$, ** $P < .01$, *** $P < .001$, **** $P < .0001$.

Numerous studies have demonstrated that the occurrence and progression of HCC involve various well-established biological mechanisms, including EMT, tumor-mesenchymal interaction, tumor microenvironment, tumor stem cells, dysregulated microRNAs, and known signaling pathways [23]. At the cellular level, uncontrolled cell proliferation and DNA replication are prominent features of cancer, triggered by DNA helicase catalysis. Therefore, in-depth exploration of these distinct molecular events is essential for understanding their underlying causes and identifying potential therapeutic targets. In this context, CDC45, a crucial constituent of the CMG complex involved in unwinding double-stranded DNA, plays a pivotal role in regulating the initiation and elongation stages of eukaryotic DNA replication [14]. The deletion or dysfunction of CDC45 leads to cell proliferation inhibition and even cell death [24,25]. Recently, some bioinformatics studies have observed that CDC45 expression is significantly up-regulated in most cancers, showing a significant negative correlation with overall survival. As an illustration, Hu et al. discovered that CDC45 gene expression was amplified in colorectal cancer based on profile analysis, establishing its use as an independent prognostic indicator in the disease [26]. Similarly, Huang et al. demonstrated a positive association between CDC45 and NSCLC by drawing on co-expression network analysis and functional evaluation. Moreover, down-regulating CDC45 expression suppressed the proliferation of NSCLC cells *in vitro* and *in vivo* by interfering with cell division at the G2/M phase, thus providing evidence supporting the oncogenic role of CDC45 [16]. Additionally, Lu et al. investigated the relationship between CDC45 and genomic alterations, tumor-infiltrating immune cells, m6A methylation, and cancer survival. These findings suggest that CDC45 may be a potential biomarker and target for cancer treatment [27]. CDC45 expression is heightened in HCC, with elevated levels and genetic alterations potentially linked to poorer prognosis in patients [19,28]. Specifically, in HCC, a subpopulation of liver cancer cells endowed with stem-like properties contributes significantly to the unfavorable prognosis observed in patients [29]. These cancer stem cells drive disease progression, confer resistance to chemotherapy, and impact the effectiveness of treatments due to their ability to generate tumors from

small numbers of cells [30,31]. Importantly, glycolysis is a heavily implicated process in the maintenance of cancer stem cell-like states in some cancer cells, emphasizing its role in metabolic reprogramming [32–34]. Fan et al. confirmed that KCNN4 promotes HCC stemness and progression by enhancing glycolysis [35]. Zhan et al. reported that SNRPB can induce HCC metabolic reprogramming, increase aerobic glycolysis, and drive HCC stemness [36]. CDC45 serves as a significant biomarker for HCC stemness [18]. Despite this, the specific manner in which CDC45 relates to HCC remains poorly understood. In our research endeavors, we determined that CDC45 overexpression correlates significantly to poorer outcomes in HCC patients. Additionally, knockdown of CDC45 was found to impede HCC cell invasion, migration, proliferation, EMT, glycolysis, and cell stemness, while promoting apoptosis.

Proteins (methyltransferase, demethylase, and binding protein) responsible for m6A modification promote or inhibit cancer, influencing cancer progression and patient prognoses [37]. For instance, Shi et al. observed that miR210HG promotes breast cancer advancement through IGF2BP1-mediated m6A modification [38]. Furthermore, Chen et al. discovered that METTL3 prompts colorectal cancer progression by impeding anti-tumor immunity via the m6A-Bhlhe41-Cxcl1/Cxcr2 pathway [39]. In contrast, Zhu et al. found that METTL3 facilitates m6A modification of STEAP2 mRNA in papillary thyroid carcinoma, thereby inhibiting the disease's progression [40]. Similarly, there seem to be distinct patterns of m6A-related gene expression in HCC and normal tissues, with such genes potentially impacting HCC prognosis [8,41]. IGF2BP2, a m6A reader, is involved in the advancement of cancers such as breast cancer [42], colorectal cancer [43], glioma [44], lung cancer [45], pancreatic cancer [46], by interacting with various RNAs including miRNAs, mRNAs, and lncRNAs [47]. Pu et al. found that IGF2BP2 is overexpressed in HCC tissues and is associated with poor prognosis. They also discovered that IGF2BP2 stabilizes FEN1 mRNA through m6A-dependent binding, promoting HCC proliferation in both *in vitro* and *in vivo* models. These findings suggest that IGF2BP2 may function as an oncogene and have the potential to serve as a biomarker for prognostic prediction in HCC

[12]. In addition, Wei et al. also found that IGF2BP2 recognizes 10 key MIRDEGs through m6A modification and stabilizes their mRNA, resulting in the up-regulation of these genes, which will disrupt the normal cell cycle, change the tumor microenvironment, and promote HCC progression [48]. Cancer metabolic reprogramming, especially aerobic glycolysis, has become a hallmark of cancer progression [9]. It has been reported that the metabolic reprogramming of HCC cells is induced by HBXIP, which mediates m6A modification of HIF-1 α through METTL3 [10]. Another study reported that CircRHBD1 enhances HCC glycolysis and limits the efficacy of immunotherapy by promoting m6A reader YTHDF1-mediated PIK3R1 translation [11]. Nevertheless, the influence of IGF2BP2 on the glycolysis process of HCC is yet to be ascertained by research. In our study, we noted that IGF2BP2 impacted CDC45 mRNA stability. Furthermore,

overexpressing IGF2BP2 served to enhance HCC cell glycolysis, stemness, invasion, migration, proliferation, and impede apoptosis, which was reversed upon CDC45 knockdown.

In the past decade, immuno oncology has undergone a paradigm shift in the treatment of malignant tumors, including HCC. Immunotherapy for HCC primarily encompasses immune checkpoint inhibitors (ICIs), cytokine therapy, tumor vaccines, and immune cell therapies. Among these, various ongoing clinical trials, particularly those involving ICIs, have provided increasing medical evidence for the clinical application of HCC immunotherapy [49,50]. A meta-analysis revealed that ICIs significantly improved overall survival, progression-free survival, and overall response rate in HCC patients compared to standard therapy [51]. Previous studies have demonstrated a positive or negative correlation between CDC45 and

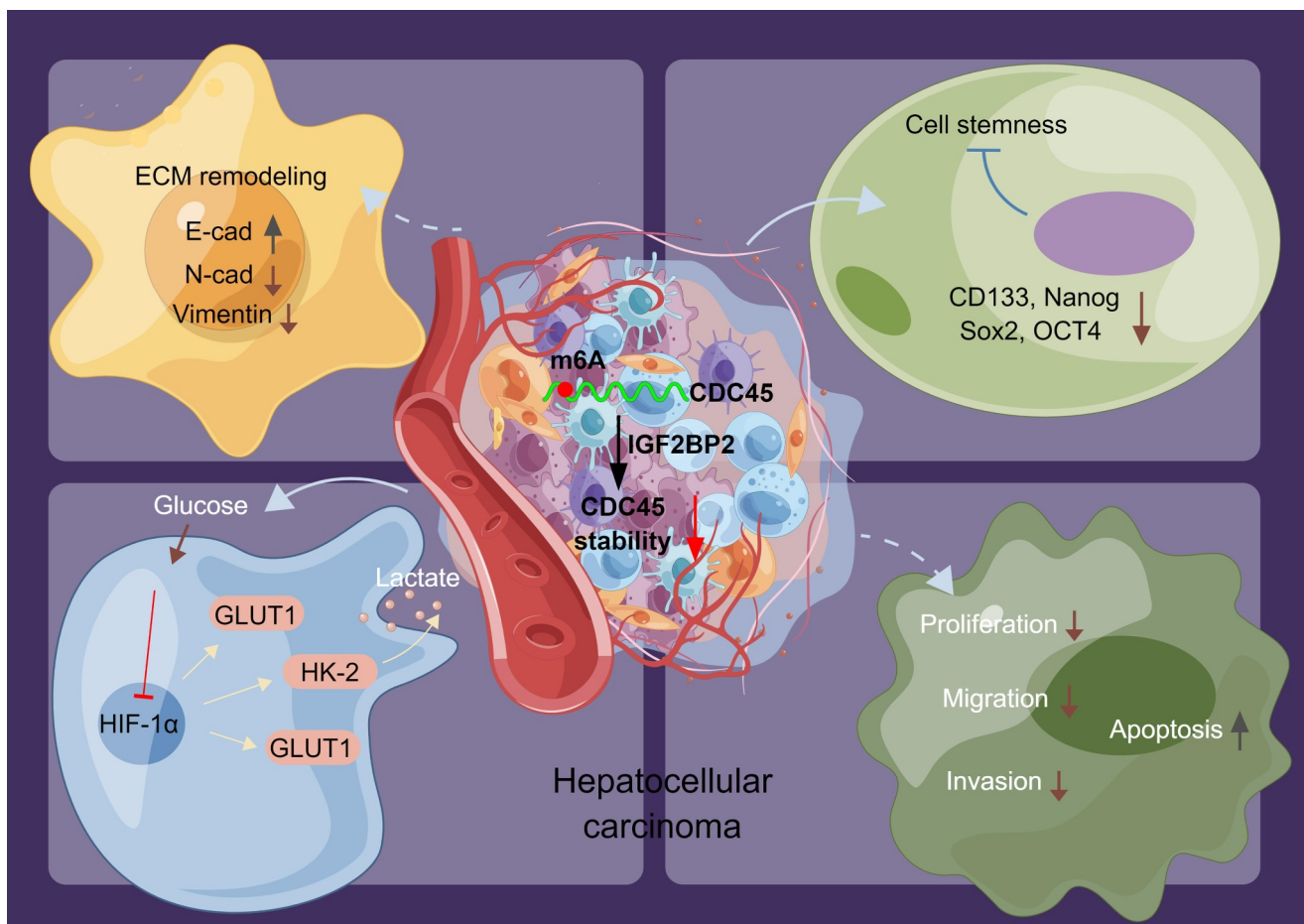


Figure 8. Graphical abstract of this study IGF2BP2 promoted glycolysis and hepatocellular carcinoma stemness by conferring stability on CDC45 mRNA through m6A modification.

immune cells in various cancer types. Additionally, in certain cancers, CDC45 expression has been observed to positively correlate with microsatellite instability and the expression of nascent antigens, indicating an association between CDC45 and the immunological characteristics of diverse tumors [27]. He et al. also explored the association between CDC45 expression and tumor infiltrating immune cells in cervical cancer, discovering a close relationship with specific subsets of immune cells [52]. Consequently, it is crucial to conduct further investigation into the relationship between CDC45 expression and immune checkpoint molecules (such as PD-L1) or immune cell infiltration patterns, as well as the impact of CDC45 expression on the immunophenotype of HCC tumors. This will help us gain a comprehensive understanding of the potential of CDC45 in HCC immunotherapy. Moreover, considering the influence of CDC45 on glycolysis and cancer stemness, investigating the effects of these cellular processes on the immunogenicity of HCC cells would be of significant interest. Additionally, delving into the immune regulatory role of CDC45 in antigen presentation, T cell activation, and tumor immune evasion mechanisms would provide vital insights into the potential synergy between CDC45-targeted therapy and immunotherapy approaches.

Conclusion

This research centers on investigating the function and mechanism of CDC45 in HCC, employing bioinformatics analysis, *in vivo*, and *in vitro* experiments (Figure 8). Our findings indicated that IGF2BP2 promoted glycolysis and hepatocellular carcinoma stemness by conferring stability on CDC45 mRNA through m6A modification. Our findings suggest that CDC45 holds potential as a promising biomarker and therapeutic target for HCC. However, it is important to acknowledge the limitations of this study. Firstly, due to feasibility and resource constraints, we opted for a small sample size in our animal experiments, which may introduce certain limitations. Therefore, in future research, we plan to expand the sample size to ensure the

reliability and generalizability of the results. Additionally, given the increasing importance of immunotherapy in HCC treatment, it would be intriguing to investigate the potential interaction between CDC45 and immunotherapy strategies in HCC. Nevertheless, it is crucial to note that the current study primarily relied on the nude mouse model, which lacks an immune system and fails to replicate the complex interactions of immune cells within the human body and the impact of immunotherapy. In subsequent studies, we aim to employ HCC allogeneic mouse models that form tumors in immunocompetent mouse strains to more accurately assess the interaction between CDC45 and immunotherapy strategies, providing more valuable insights.

Acknowledgements

The work was supported by funds from Hainan Provincial Key Laboratory of Tumorigenesis Intervention, Open Project Fund (JCKF2021006). The graphic abstract was drawn using Figdraw (www.figdraw.com).

Disclosure statement

No potential conflict of interest was reported by the author(s).

Funding

The work was supported by the Hainan Provincial Key Laboratory of Tumorigenesis Intervention, Open Project Fund [JCKF2021006].

References

- [1] Ganesan P, Kulik LM. Hepatocellular Carcinoma: New Developments. *Clin Liver Dis.* 2023;27(1):85–102. doi: [10.1016/j.cld.2022.08.004](https://doi.org/10.1016/j.cld.2022.08.004)
- [2] Rungay H, Arnold M, Ferlay J, et al. Global burden of primary liver cancer in 2020 and predictions to 2040. *J Hepatol.* 2022;77(6):1598–1606. doi: [10.1016/j.jhep.2022.08.021](https://doi.org/10.1016/j.jhep.2022.08.021)
- [3] Sung H, Ferlay J, Siegel RL, et al. Global cancer statistics 2020: GLOBOCAN estimates of incidence and mortality worldwide for 36 cancers in 185 countries. *CA Cancer J Clin.* 2021;71(3):209–249. doi: [10.3322/caac.21660](https://doi.org/10.3322/caac.21660)
- [4] Nagaraju GP, Dariya B, Kasa P, et al. Epigenetics in hepatocellular carcinoma. *Semin Cancer Biol.* 2022;86:622–632. doi: [10.1016/j.semcancer.2021.07.017](https://doi.org/10.1016/j.semcancer.2021.07.017)

- [5] Ouyang W, Wang MD, Wang WY, et al. Hydroxymethylation and Epigenetic drugs: new insights into the diagnosis and treatment in epigenetics of hepatocellular carcinoma. *J Oncol.* 2023;2023:5449443. doi: [10.1155/2023/5449443](https://doi.org/10.1155/2023/5449443)
- [6] Bouyahya A, Mechchate H, Oumeslakht L, et al. The role of Epigenetic Modifications in human cancers and the use of natural compounds as Epidrugs: mechanistic pathways and pharmacodynamic actions. *Biomolecules.* 2022;12(3):12. doi: [10.3390/biom12030367](https://doi.org/10.3390/biom12030367)
- [7] Sun T, Wu R, Ming L. The role of m6A RNA methylation in cancer. *Biomed Pharmacother.* 2019;112:108613. doi: [10.1016/j.biopha.2019.108613](https://doi.org/10.1016/j.biopha.2019.108613)
- [8] Huang H, Bai Y, Lu X, et al. N6-methyladenosine associated prognostic model in hepatocellular carcinoma. *Ann Transl Med.* 2020;8(10):633. doi: [10.21037/atm-20-2894](https://doi.org/10.21037/atm-20-2894)
- [9] Yao H, Yang F, Li Y. Natural products targeting human lactate dehydrogenases for cancer therapy: a mini review. *Front Chem.* 2022;10:1013670. doi: [10.3389/fchem.2022.1013670](https://doi.org/10.3389/fchem.2022.1013670)
- [10] Yang N, Wang T, Li Q, et al. HBXIP drives metabolic reprogramming in hepatocellular carcinoma cells via METTL3-mediated m6A modification of HIF-1 α . *J Cell Physiol.* 2021;236(5):3863–3880. doi: [10.1002/jcp.30128](https://doi.org/10.1002/jcp.30128)
- [11] Cai J, Chen Z, Zhang Y, et al. CircRHBDD1 augments metabolic rewiring and restricts immunotherapy efficacy via m(6)A modification in hepatocellular carcinoma. *Mol Ther Oncolytics.* 2022;24:755–771. doi: [10.1016/j.omto.2022.02.021](https://doi.org/10.1016/j.omto.2022.02.021)
- [12] Pu J, Wang J, Qin Z, et al. IGF2BP2 promotes liver cancer growth through an m6A-FEN1-Dependent mechanism. *Front Oncol.* 2020;10:578816. doi: [10.3389/fonc.2020.578816](https://doi.org/10.3389/fonc.2020.578816)
- [13] Chen C, Chen S, Pang L, et al. Analysis of the expression of cell division cycle-associated genes and its prognostic significance in human lung carcinoma: A review of the literature databases. *Biomed Res Int.* 2020;2020:1–14. doi: [10.1155/2020/6412593](https://doi.org/10.1155/2020/6412593)
- [14] Seo YS, Kang YH. The human replicative helicase, the CMG complex, as a target for anti-cancer therapy. *Front Mol Biosci.* 2018;5:26. doi: [10.3389/fmolb.2018.00026](https://doi.org/10.3389/fmolb.2018.00026)
- [15] Shen H, Guo YL, Li GH, et al. Gene expression analysis reveals key genes and Signalings associated with the prognosis of prostate cancer. *Comput Math Methods Med.* 2021;2021:9946015. doi: [10.1155/2021/9946015](https://doi.org/10.1155/2021/9946015)
- [16] Huang J, Li Y, Lu Z, et al. Analysis of functional hub genes identifies CDC45 as an oncogene in non-small cell lung cancer - a short report. *Cell Oncol.* 2019;42(4):571–578. doi: [10.1007/s13402-019-00438-y](https://doi.org/10.1007/s13402-019-00438-y)
- [17] Yang S, Ren X, Liang Y, et al. KNK437 restricts the growth and metastasis of colorectal cancer via targeting DNAJA1/CDC45 axis. *Oncogene.* 2020;39(2):249–261. doi: [10.1038/s41388-019-0978-0](https://doi.org/10.1038/s41388-019-0978-0)
- [18] Zhao Z, Mu H, Feng S, et al. Identification of biomarkers associated with hepatocellular carcinoma stem cell characteristics based on co-expression network analysis of Transcriptome data and stemness Index. *Crit Rev Eukaryot Gene Expr.* 2022;32(2):47–60. doi: [10.1615/CritRevEukaryotGeneExpr.2021039692](https://doi.org/10.1615/CritRevEukaryotGeneExpr.2021039692)
- [19] Lu HP, Du XF, Li JD, et al. Expression of cell division cycle protein 45 in tissue microarrays and the CDC45 gene by bioinformatics analysis in human hepatocellular carcinoma and patient outcomes. *Med Sci Monit.* 2021;27:e928800. doi: [10.12659/MSM.928800](https://doi.org/10.12659/MSM.928800)
- [20] Yao B, Li Y, Niu Y, et al. Hypoxia-induced miR-3677-3p promotes the proliferation, migration and invasion of hepatocellular carcinoma cells by suppressing SIRT5. *J Cell Mol Med.* 2020;24(15):8718–8731. doi: [10.1111/jcmm.15503](https://doi.org/10.1111/jcmm.15503)
- [21] Bi L, Ren Y, Feng M, et al. HDAC11 regulates glycolysis through the LKB1/AMPK signaling pathway to maintain hepatocellular carcinoma stemness. *Cancer Res.* 2021;81(8):2015–2028. doi: [10.1158/0008-5472.CAN-20-3044](https://doi.org/10.1158/0008-5472.CAN-20-3044)
- [22] Wang Q, Xie H, Peng H, et al. ZC3H13 inhibits the progression of hepatocellular carcinoma through m(6)A-PKM2-Mediated glycolysis and enhances chemosensitivity. *J Oncol.* 2021;2021:1328444. doi: [10.1155/2021/1328444](https://doi.org/10.1155/2021/1328444)
- [23] Ogunwobi OO, Harricharran T, Huaman J, et al. Mechanisms of hepatocellular carcinoma progression. *World J Gastroenterol.* 2019;25(19):2279–2293. doi: [10.3748/wjg.v25.i19.2279](https://doi.org/10.3748/wjg.v25.i19.2279)
- [24] Yadav A, Sharma V, Pal J, et al. DNA replication protein Cdc45 directly interacts with PCNA via its PIP box in *Leishmania donovani* and the Cdc45 PIP box is essential for cell survival. *PLOS Pathog.* 2020;16(5):e1008190. doi: [10.1371/journal.ppat.1008190](https://doi.org/10.1371/journal.ppat.1008190)
- [25] Sun J, Shi R, Zhao S, et al. Cell division cycle 45 promotes papillary thyroid cancer progression via regulating cell cycle. *Tumour Biol.* 2017;39(5):1010428317705342. doi: [10.1177/1010428317705342](https://doi.org/10.1177/1010428317705342)
- [26] Hu Y, Wang L, Li Z, et al. Potential prognostic and Diagnostic Values of CDC6, CDC45, ORC6 and SNHG7 in colorectal cancer. *Onco Targets Ther* 2019; 12: 11609–11621. doi: [10.2147/OTT.S231941](https://doi.org/10.2147/OTT.S231941).
- [27] Lu Y, Chen X, Liu F, et al. Systematic pan-cancer analysis identifies CDC45 as having an oncogenic role in human cancers. *Oncol Rep.* 2022;48(4):48. doi: [10.3892/or.2022.8400](https://doi.org/10.3892/or.2022.8400)
- [28] Xiang XH, Yang L, Zhang X, et al. Seven-senescence-associated gene signature predicts overall survival for Asian patients with hepatocellular carcinoma. *World J Gastroenterol.* 2019;25(14):1715–1728. doi: [10.3748/wjg.v25.i14.1715](https://doi.org/10.3748/wjg.v25.i14.1715)
- [29] Cai JL, Zhu GQ, Du JX, et al. Identification and validation of a new gene signature predicting prognosis of hepatocellular carcinoma patients by network analysis of stemness indices. *Expert Rev Gastroenterol Hepatol.* 2021;15(6):699–709. doi: [10.1080/17474124.2021.1845142](https://doi.org/10.1080/17474124.2021.1845142)

- [30] Espinosa-Sánchez A, Suárez-Martínez E, Sánchez-Díaz L, et al. Therapeutic targeting of signaling pathways related to cancer stemness. *Front Oncol.* 2020;10:1533. doi: [10.3389/fonc.2020.01533](https://doi.org/10.3389/fonc.2020.01533)
- [31] Lee HY, Hong IS. Targeting liver cancer stem cells: an alternative therapeutic approach for liver cancer. *Cancers (Basel).* 2020;12(10):12. doi: [10.3390/cancers12102746](https://doi.org/10.3390/cancers12102746)
- [32] Nwosu ZC, Piorońska W, Battello N, et al. Severe metabolic alterations in liver cancer lead to ERK pathway activation and drug resistance. *EBioMedicine.* 2020;54:102699. doi: [10.1016/j.ebiom.2020.102699](https://doi.org/10.1016/j.ebiom.2020.102699)
- [33] Gnocchi D, Sabbà C, Massimi M, et al. Metabolism as a New Avenue for hepatocellular carcinoma therapy. *Int J Mol Sci.* 2023;24(4):24. doi: [10.3390/ijms24043710](https://doi.org/10.3390/ijms24043710)
- [34] Chen YY, Wang WH, Che L, et al. BNIP3L-Dependent mitophagy promotes HBx-induced cancer stemness of hepatocellular carcinoma cells via glycolysis metabolism reprogramming. *Cancers (Basel).* 2020;12(3):12. doi: [10.3390/cancers12030655](https://doi.org/10.3390/cancers12030655)
- [35] Fan J, Tian R, Yang X, et al. KCNN4 promotes the stemness potentials of liver cancer stem cells by enhancing glucose metabolism. *Int J Mol Sci.* 2022;23(13):23. doi: [10.3390/ijms23136958](https://doi.org/10.3390/ijms23136958)
- [36] Zhan YT, Li L, Zeng TT, et al. SNRPB-mediated RNA splicing drives tumor cell proliferation and stemness in hepatocellular carcinoma. *Aging.* 2020;13(1):537–554. doi: [10.18632/aging.202164](https://doi.org/10.18632/aging.202164)
- [37] Wei Y, Li Y, Lu C. Exploring the role of m6A modification in cancer. *Proteomics.* 2022;23(13–14):e2200208. doi: [10.1002/pmic.202200208](https://doi.org/10.1002/pmic.202200208)
- [38] Shi W, Tang Y, Lu J, et al. MIR210HG promotes breast cancer progression by IGF2BP1 mediated m6A modification. *Cell Biosci.* 2022;12(1):38. doi: [10.1186/s13578-022-00772-z](https://doi.org/10.1186/s13578-022-00772-z)
- [39] Chen H, Pan Y, Zhou Q, et al. METTL3 inhibits anti-tumor immunity by targeting m(6)A-BHLHE41-CXCL1/CXCR2 axis to promote colorectal cancer. *Gastroenterology.* 2022;163(4):891–907. doi: [10.1053/j.gastro.2022.06.024](https://doi.org/10.1053/j.gastro.2022.06.024)
- [40] Zhu Y, Peng X, Zhou Q, et al. METTL3-mediated m6A modification of STEAP2 mRNA inhibits papillary thyroid cancer progress by blocking the hedgehog signaling pathway and epithelial-to-mesenchymal transition. *Cell Death Dis.* 2022;13(4):358. doi: [10.1038/s41419-022-04817-6](https://doi.org/10.1038/s41419-022-04817-6)
- [41] Wang Y, Li T, Liu H, et al. N6-methyladenosine methylation-related genes YTHDF2, METTL3, and ZC3H13 predict the prognosis of hepatocellular carcinoma patients. *Ann Transl Med.* 2022;10(24):1398. doi: [10.21037/atm-22-5964](https://doi.org/10.21037/atm-22-5964)
- [42] Gao C, Li L, Jin X, et al. The involvement of insulin-like growth factor 2 Messenger ribonucleic acid-binding protein 2 in the Regulation of the expression of breast cancer-related genes. *Breast Cancer (Dove Med Press).* 2022;14:311–322. doi: [10.2147/BCTT.S382566](https://doi.org/10.2147/BCTT.S382566)
- [43] Bian Y, Wang Y, Xu S, et al. m(6)A modification of long non-coding RNA HNF1A-AS1 facilitates cell cycle progression in colorectal cancer via IGF2BP2-mediated CCND1 mRNA stabilization. *Cells.* 2022;11(19):11. doi: [10.3390/cells11193008](https://doi.org/10.3390/cells11193008)
- [44] Guan S, He Y, Su Y, et al. A risk signature consisting of eight m(6)A methylation regulators predicts the prognosis of glioma. *Cell Mol Neurobiol.* 2022;42(8):2733–2743. doi: [10.1007/s10571-021-01135-x](https://doi.org/10.1007/s10571-021-01135-x)
- [45] Yang J, Qian X, Qiu Q, et al. LCAT1 is an oncogenic lncRNA by stabilizing the IGF2BP2-CDC6 axis. *Cell Death Dis.* 2022;13(10):877. doi: [10.1038/s41419-022-05316-4](https://doi.org/10.1038/s41419-022-05316-4)
- [46] Zhan J, Zhang Q, Tong X, et al. HNF4G stimulates the development of pancreatic cancer by promoting IGF2BP2 transcription. *Clin Transl Oncol.* 2023;25(5):1472–1481. doi: [10.1007/s12094-022-03048-7](https://doi.org/10.1007/s12094-022-03048-7)
- [47] Wang J, Chen L, Qiang P. The role of IGF2BP2, an m6A reader gene, in human metabolic diseases and cancers. *Cancer Cell Int.* 2021;21(1):99. doi: [10.1186/s12935-021-01799-x](https://doi.org/10.1186/s12935-021-01799-x)
- [48] Wei Q. Bioinformatical identification of key genes regulated by IGF2BP2-mediated RNA N6-methyladenosine and prediction of prognosis in hepatocellular carcinoma. *J Gastrointest Oncol.* 2021;12(4):1773–1785. doi: [10.21037/jgo-21-306](https://doi.org/10.21037/jgo-21-306)
- [49] Yu SJ. Immunotherapy for hepatocellular carcinoma: recent advances and future targets. *Pharmacol Ther.* 2023;244:108387. doi: [10.1016/j.pharmthera.2023.108387](https://doi.org/10.1016/j.pharmthera.2023.108387)
- [50] Sangro B, Sarobe P, Hervás-Stubbis S, et al. Advances in immunotherapy for hepatocellular carcinoma. *Nat Rev Gastroenterol Hepatol.* 2021;18(8):525–543. doi: [10.1038/s41575-021-00438-0](https://doi.org/10.1038/s41575-021-00438-0)
- [51] Guven DC, Erul E, Sahin TK, et al. The benefit of immunotherapy in patients with hepatocellular carcinoma: a systematic review and meta-analysis. *Future Oncol.* 2022;18(37):4119–4136. doi: [10.2217/fon-2022-0642](https://doi.org/10.2217/fon-2022-0642)
- [52] He Z, Wang X, Yang Z, et al. Expression and prognosis of CDC45 in cervical cancer based on the GEO database. *PeerJ.* 2021;9:e12114. doi: [10.7717/peerj.12114](https://doi.org/10.7717/peerj.12114)